

## Influence of Plastic Deformation on Recrystallized Microstructure of Fe-Base Ods Alloy

C. Capdevila\*, I. Toda-Caraballo, G. Pimentel, and J. Chao

Department of Physical Metallurgy, Centro Nacional de Investigaciones Metalúrgicas (CENIM - CSIC),  
Avda. Gregorio del Amo, 8. E-28040 Madrid, Spain

(received date: 11 August 2011 / accepted date: 19 December 2011)

The ferritic oxide dispersion strengthened alloys (ODS) are manufactured using the mechanical alloying process. The development of a coarse grained microstructure during recrystallization has been noted and discussed by a number of authors, but the mechanism of grain control remains uncertain. Recent work has emphasized the large influence of non-uniformities on the development of the recrystallized microstructure. The purpose of the present work was to study, with the help of finite element modeling techniques, the effect of non-uniform plastic strain on recrystallization of Fe-base ODS alloy named MA 957.

**Key words:** metals, hot isostatic pressing, thermomechanical processing, recrystallization, electron backscattering diffraction

### 1. INTRODUCTION

The ferritic ODS alloy discussed in this paper was obtained using mechanical alloying [1-4]. This introduces a uniform distribution of fine oxide particles, which provide resistance to creep deformation at elevated temperatures. As the ferritic state makes the alloy resistant to radiation induced swelling, MA957 was intended for the manufacture of tubes for nuclear reactor applications, to contain liquid sodium at about 700 °C [5].

The alloy, after consolidation from the powder, has a high stored energy, due to deformation and the small grain size. The energy is typically 1 J g<sup>-1</sup>, which is much greater than in conventionally deformed metals [6]. It is therefore peculiar that the consolidated alloy has to be heated to temperatures as high as 1400 °C before recrystallization begins [7]. An important observation by Regle and Alamo [8] is that the recrystallization temperature dramatically decreases if the consolidated material is cold-deformed prior to annealing. This observation has been confirmed in the works carried out by Capdevila *et al.* [2-4] in other Fe-base mechanically alloyed materials. It appears that two factors, the peculiar distribution of high- (HAGB) and low- (LAGB) angle grain boundaries in the as-consolidated state, and the uniformity of the fine scale microstructure, make the nucleation of recrystallization difficult, because the grain boundary junctions are strong pinning points, restricting the bowing of grain bound-

aries [7]. In effect, the fine grains cannot be considered topologically independent, as is assumed in recrystallization models. In these circumstances, anything that introduces inhomogeneity into the microstructure will ameliorate the recrystallization process, explaining the Regle and Alamo results.

In the present work, we examine the effect of deforming the compacted material on the development of the recrystallization grain structure using bend samples in MA957, where there is not only a deformation gradient about the neutral axis but also a change in the sign of the plastic strain. The microstructural analysis is compared with the information obtained by FEM simulations in terms of distribution of stresses and strain energy density.

### 2. EXPERIMENTAL PROCEDURES

MA957 (Fe-0.01C-14Cr-1Ti-0.3Mo-0.27Y<sub>2</sub>O<sub>3</sub>) was fabricated by charging three primary powders (elemental iron, pre-alloyed metallic alloys, and yttria) into a water-cooled vertical attritor for mechanical alloying. The consolidation of the resultant powder was achieved by extrusion at 1000 °C, while packed in a mild steel can. This was followed by rolling at 1000 °C, to reduce the bar diameter from 54 to 25 mm. The final microstructure is in a cold deformed state and presents a grain size of 0.4 μm in average diameter.

The bend test samples were 100 mm length, machined parallel to the bar axis (extrusion direction or TD), and square in cross-section (7×7 mm<sup>2</sup>). Bending was carried out using a MAYES-100 kN. Samples were etched for optical

\*Corresponding author: ccm@cenim.csic.es  
©KIM and Springer, Published 10 October 2012

microscopy using 2 g CuCl<sub>2</sub>, 40 ml HCl, and 40-80 ml ethanol.

Microtexture analysis of specimens was performed by the Electron Backscattering Diffraction (EBSD) technique. The EBSD patterns were generated at an acceleration voltage of 20 kV and collected using a CRYSTAL detector of Oxford Instruments mounted in a FEG-SEM JEOL JSM6500. The indexation of the Kikuchi lines and the determination of the orientations were done with the software CHANNEL 5 developed by HKL Technologies. The results were represented by means of {100}-pole figures which show the stereographic projection of {100} planes in the crystals onto the longitudinal section of the sample. For all samples, the plane investigated by EBSD was the one containing the bar axis (TD) and the radial direction (RD).

In order to discern the effect of the plastic strain and stress distribution on the recrystallization, a Finite Element Modeling (FEM) was performed by the Multiphysics Modeling and Simulation Software COMSOL. The results were analyzed comparing the aspect of the recrystallized zones with those of the iso-strain and iso-stress contours following the Von Mises criterion, since Von Mises stress is isotropic and is related to dislocation glide. The simulations were performed considering the three-point bend test with a cylinder of 5 mm in radius acting as a plunger with isotropic linear elastic behavior. The contact between plunger and sample was modeled as Coulomb friction with a friction coefficient of 0.1. The load considered in calculations was 11 kN. Simulations were performed on rectangular sample 7×7 mm<sup>2</sup> in section and 100 mm in length, considering a 2D mesh with planar symmetry with the plane normal to the bar axis (TD). Due to the axial symmetry of the specimen with respect to the punch direction, only one half of the bending specimen was considered in FEM simulations. Nevertheless, for the sake of clarity, the results are presented on the complete specimen. The sample was modeled as an elastoplastic material with isotropic Von Mises yield criterion and with isotropic work hardening in which the Young's modulus was 210 GPa and the Poisson's ratio was 0.3.

Of particular interest is the state of deformation at the temperature when recrystallization is triggered. At this state the residual stresses of the unloaded state are allowed to move and relax. For this reason, the residual stress evolution (function of the initial unloaded state and temperature) during recrystallization heat treatment, has been analyzed using the finite element method and the constitutive equation proposed by Johnson - Cook [9]. In this sense, the evolution of the stress - strain curve with temperature could be expressed as follows:

$$\sigma = (A + B\bar{\epsilon}_p^n) \left( 1 + C \ln \frac{\dot{\epsilon}_p}{\dot{\epsilon}_0} \right) \left( 1 - \left( \frac{T - T_r}{T_m - T_r} \right)^m \right) \quad (1)$$

The parameters  $A = 1000$ ,  $B = 865.7$ , and  $n = 0.505$  are

those defining the experimental stress-strain curve for MA 957,  $C$  is the strain-rate coefficient considered to be  $1.5 \times 10^{-2}$  [10],  $\dot{\epsilon}_0$  is the initial plastic strain rate with a reference value of  $10^{-4} \text{ s}^{-1}$  and  $\dot{\epsilon}_p$  is the plastic strain rate. The effect of the temperature is defined through  $T$  (current temperature),  $T_r$  (room temperature, *i.e.* 25 °C),  $T_m$  (melting temperature, *i.e.* 1478 °C) and the thermal softening constant ( $m$ ) considered to be 0.6 [11]. Moreover, the negligible effect of Young's modulus temperature dependence was checked by calculations.

### 3. RESULTS AND DISCUSSION

Figure 1 shows the form of the bend test samples and Table 1 summarizes the experimental parameters. The thickness of the layer of yielded material increases with the bending moment  $M$ , so that the elastic-plastic boundary approaches the neutral axis as  $M$  becomes larger. The moment  $M_p$  required to make the section fully plastic is given by Johnson and Mellor [12] to be where  $w$  and  $h$  are the width and height respectively of the square section of the sample. A yield stress ( $\sigma_0$ ) of 1125 MPa was experimentally determined by tensile testing. For the dimensions of the samples used in this work  $M_p = 96 \text{ N m}$ .

Recrystallization in iron-base ODS alloys occurs at exceptionally high temperatures, of the order of 0.9 of the melting temperature (in MA957  $T_m = 1478 \text{ C}$ ). As shown in Fig. 2, the minimum temperature at which the material recrystallizes after 1 h has been measured for MA957 to be  $T_R = 1330 \text{ °C}$ . In order to characterize the effect of deformation on the recrystallization temperature, heat treatments were carried

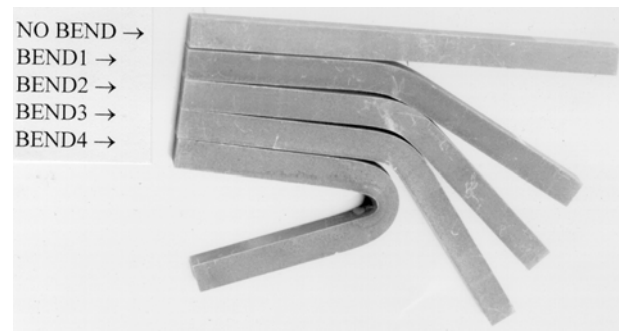


**Fig. 1.** Bend samples. The parameters of the bending are summarized in Table 1.

**Table 1.** Bend test parameters

	d / mm	F / kN	M / Nm
Bend1	9.23	6.2	71
Bend2	15.57	6.07	70
Bend3	16.81	6.9	80
Bend4	41.12	10.1	115

d stands for displacement; F stands for maximum load; M stands for bend moment.

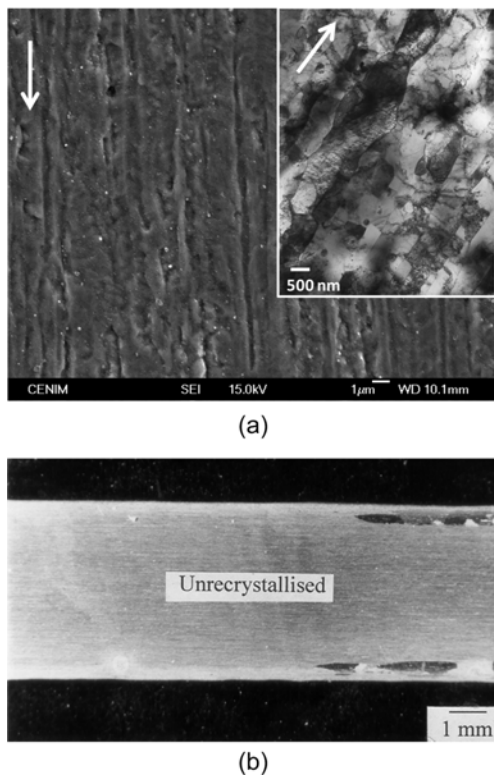


**Fig. 2.** Longitudinal section of unbend sample (a) in the as-hot rolled condition (arrow indicate the extrusion direction), and (b) recrystallized at  $T_R$  temperature ( $T_R = 1330\text{ }^\circ\text{C}$ ).

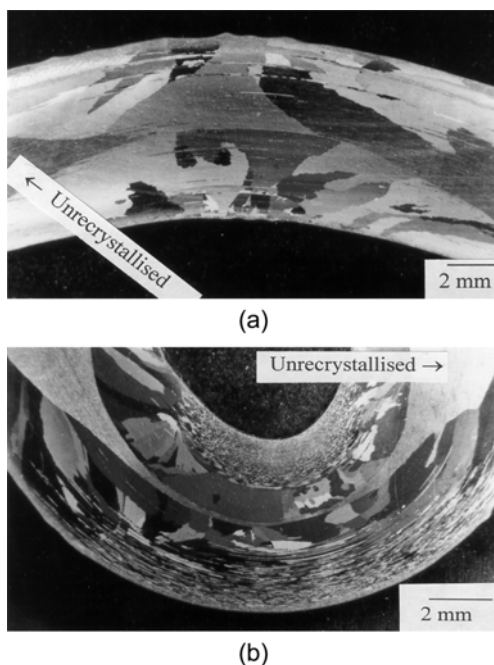


**Fig. 3.** Longitudinal section of (a) sample Bend 2 and (b) sample Bend 4 recrystallized at ( $T_R - 30\text{ }^\circ\text{C}$ ) for 1 h.

out on the bent samples at temperatures lower than  $T_R$ . Fig. 3 shows the microstructures of samples Bend 2 and Bend 4

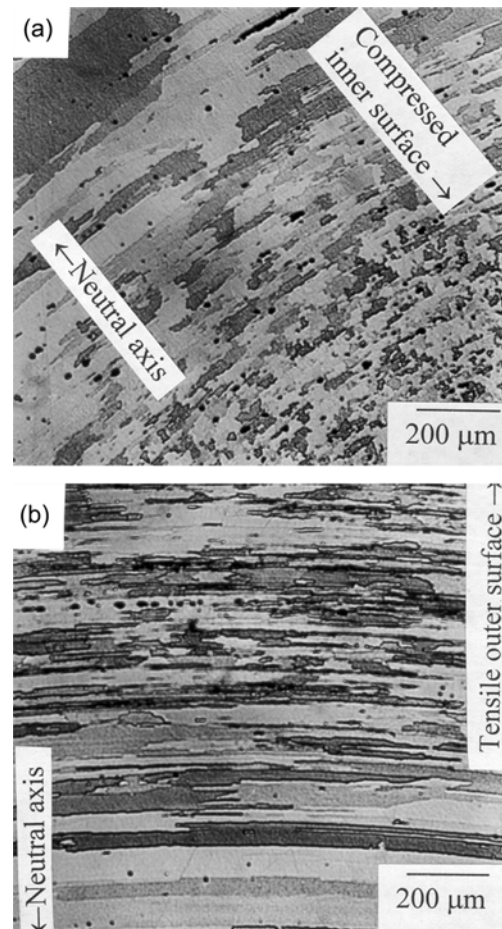


**Fig. 4.** Detailed view of (a) compressed, and (b) tensile regions of sample Bend 4.

after deformation and recrystallization at ( $T_R - 30\text{ }^\circ\text{C}$ ) for 1 h. The samples have almost fully recrystallized even though  $T < T_R$ . Deformation clearly decreases the minimum temperature at which recrystallization begins, and greater strain has the effect of refining the recrystallized grain structure, which is consistent with the coarser and more equiaxed areas of sample Bend 2 (Fig. 3). The grain structures in the tensile and compressed areas of sample Bend 4 are presented in Fig. 4. A finer recrystallized microstructure in the compressed area (Fig. 4(a)) as compared with the tension area (Fig. 4(b)), is obtained.

Why does a mechanically alloyed material with an enormous stored energy recrystallizes at  $0.9 T_m$ , but  $T_R$  significantly decreases with a relatively small cold deformation? A tentative explanation for this behavior will be drawn in the following paragraphs.

Immediately after the mechanical alloying process, the powders have a grain size which can be as fine as 1-2 nm locally. This is hardly surprising given the extent of the deformation during mechanical alloying, with true strains of the order of 9, equivalent to stretching a unit length by a fac-

tor of 8000. The consolidation process involves hot extrusion and rolling at temperatures of about 1000 °C, which causes recrystallization into a sub-micron grain size [2]. It is known that during the course of consolidation, the material may dynamically recrystallize several times [10]. It should be emphasized that the sub-micron grains are not low-misorientation cell structures typical in aluminum alloys, but true grains with large misorientations (Fig. 2(a)). Subsequent heat-treatment leads to recrystallization into a very coarse grained microstructure [4]. Two explanations for such behavior are presented as follows.

As it has been nicely reviewed by Klugg *et al.* [13], the recrystallization mechanisms are consistent with strain induced boundary migration (SIBM) theory. The nucleation of recrystallization in the present context begins by the bowing of a grain boundary. This normally is straightforward because the size of the boundary perturbation is small when compared with the grain size. However, with very small grains, the boundary junctions themselves act as severe pinning lines, restricting bowing. This leads to an enormous activation energy  $Q$  for the nucleation of recrystallization, ten times larger than  $Q_D$ , which is the activation energy for self diffusion [3].  $Q$  is reduced if a few grains happen to be larger; indeed, any non uniformity introduced into the microstructure will lead to a large decrease in  $T_R$  [3-4]. This is consistent with the effect of bending deformation. Because of the manufacturing process of Fe-base ODS alloys such as MA 957, the as-hot rolled microstructure is formed by higher misoriented boundary “layers” as described by Klugg *et al.* [13]. The nucleation of recrystallization takes place within those layers, which are also parallel to the plastic flow lines. Thus, these layers follow a more equiaxial pattern in the compressed area than in the tensioned area, where they are stretched by the bend moment applied. The production of a viable nucleus within the highly orientated layer could result in the rapid, orientated growth parallel to the bending plane as observed in Figs. 3 and 4.

Toda-Caraballo *et al.* [14] pointed out the role of residual shear stress triggering the recrystallization in a Fe-base ODS alloy deformed under Brinell indentation. Their results were consistent with the idea described by Hutchinson and Wynne [11] where it is described that boundary movement is accompanied by shearing of the volume through which a boundary moves. Figure 5 shows the evolution of the ratio between  $\sigma_{xy}$  and  $\tau_0$  (shear yield strength), i.e.  $\delta = \sigma_{xy}/\tau_0$  at the temperature where recrystallization was detected, by using the Johnson - Cook model. Therefore, once  $\delta$  reaches the value of one, the residual shear stress would be high enough to drive the dislocation movement, and hence to induce the movement of grain boundaries, which burst the recrystallization process. However, it is clear from Fig. 5 that  $\delta < 1$  in the whole simulated sample, which corresponds to the Bend4 sample, and obviously it is an upper bound of the samples

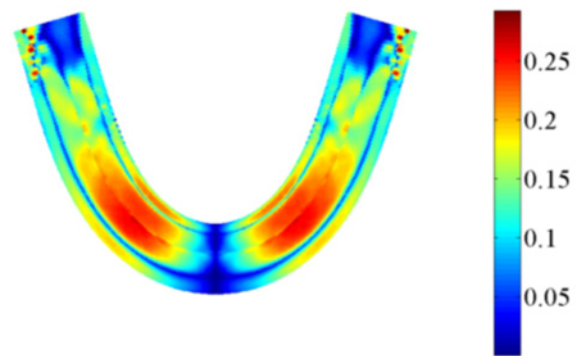


Fig. 5. Evolution of  $\delta$  at 1300 °C ( $T_R-30$  °C) for sample 4.

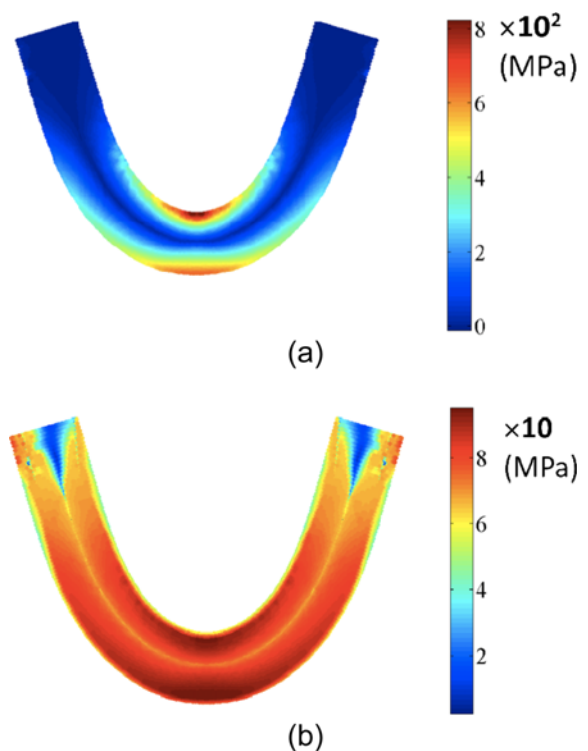


Fig. 6. (a) Strain energy density and (b) stress distribution at 1300 °C ( $T_R-30$  °C) for sample 4.

with lower loads. Therefore, in contrast to that occurring under Brinell deformation [14], the shear residual stresses are unable to drive the grain boundary motion and hence to boost recrystallization.

Nevertheless, the comparison between FEM simulation results and microstructural analysis shown in Figs. 3 and 4 clearly indicates that recrystallization is triggered in the plastically deformed areas. In this sense, Fig. 6(a) shows the distribution of plastic deformation in terms of the strain energy density at recrystallization temperature. The strain energy density represents the work done per unit volume during deformation and could be considered to be the maximum possible driving force for recrystallization at a certain tem-

perature. It is worth noting the higher values of strain energy density achieved in the compressed area, as compared with the tension areas. By contrast, the distribution of stresses at recrystallization temperature is almost uniform (Fig. 6(b)). A close relationship between strain energy distributions and recrystallization in MA 957 is found out by comparing FEM results with the microstructures shown in Figs. 3 and 4. Likewise, the higher the strain density is, the smaller the recrystallized grain size achieved.

Such behavior could be explained on the basis of a texture change induced by cold deformation. Chou [2] has measured the stored energies in the samples subjected to cold deformation after consolidation in MA 957. Surprisingly, he found no increase in stored energy with deformation; indeed, it appears that the cold deformation leads to a reduction in stored energy [15]. It could be assumed, therefore, that the cold deformation modifies the crystallographic texture. It is conceivable that the texture change both leads to a reduction in the stored energy, and at the same time, a reduction in the recrystallization temperature. The texture could, for example, lead to the clustering of adjacent grains into similar orientations. This would lead to an increase in the effective grain size, thereby making the nucleation of recrystallization easier.

Figure 7 shows the  $\{100\}$  pole figures of an as-hot rolled undeformed sample and compressed sample 4 obtained by EBSD texture measurements. The texture in the as-hot rolled unbent sample is very sharp (far from random) and is strongly dominated by one single orientation, as illustrated in Fig. 7(a). This “rotated cube” orientation is characterized by having the  $\langle 100 \rangle$ -direction (the cube edge) parallel to the radial direction (RD) and the  $\langle 110 \rangle$ -direction parallel to the bar axis direction (TD). One can obtain the orientation from a cube aligned with its edges parallel to RD and TD by applying a rotation of  $45^\circ$  around RD. Regarding the compressed area of bend sample 4, the crystal orientations are virtually random and no dominating orientations are observed, *i.e.* the texture is weak. A close examination of the contour plots does reveal, however, that the “rotated cube” orientation

which dominates the as-hot rolled unbent sample also appears here slightly more frequently than at random. In summary, while the as-hot rolled unbent material presents a strong rotated cube texture, the compressed areas present a weak texture, which indicates a bigger amount of  $\{111\}$  grains as compared with the as-hot rolled state. Therefore, it is a sensible assumption to consider that the strain energy density accumulated in the compressed area of bend sample 4 could be used to promote the formation of other texture components, among which is the  $\{111\}$  component. Published data on the correlation between crystallographic texture and recrystallization indicate that, when the cold-deformed texture is random, certain texture components grow at the expense of others during the course of recrystallization [16]. This process is similar to directional solidification, in which the fastest growing orientations are selected preferentially in the final microstructure. It is found that, during the recrystallization of cold-deformed ferritic steels, the  $\{111\}$  texture component grows preferentially [16], and a reasonable explanation for this could be that the boundary mobility of grains contributing to this particular component is relatively high. Hence it follows that, at a given value of stored energy, a sample with a stronger  $\{111\}$  texture should recrystallize more readily.

Finally the comparison of the results reported in this paper with the ones reported on the effect of Brinell hardness deformation [14] allows us to reach conclusions on the fundamental role that deformation pattern has on subsequent recrystallization. Although both bend and Brinell deformation cause a significant decrease of recrystallization temperature in Fe-base ODS alloys, the mechanism that trigger recrystallization is very different. While no texture changes were detected in the Brinell deformed samples, the nucleation of recrystallization is boosted by the residual shear stresses. On the other hand the recrystallization is triggered in the deformed samples by bending, due to the texture changes introduced during the deformation process. This is consistent with the fact that during Brinell indentation the material flow occurs homogeneously in the extrusion direction and in the same sense as that extrusion, so no texture change should be expected. By contrast, during deformation by bending the material flows in the extrusion direction but the sense of the material flow changes from tension to compression areas, which would lead a texture change in the sample.

#### 4. CONCLUSIONS

The effect of cold deformation on the recrystallization of MA957 samples is twofold. Firstly, the recrystallization temperature decreases, consistent with the hypothesis that anything that makes the original microstructure heterogeneous will encourage recrystallization. This is because the micro-

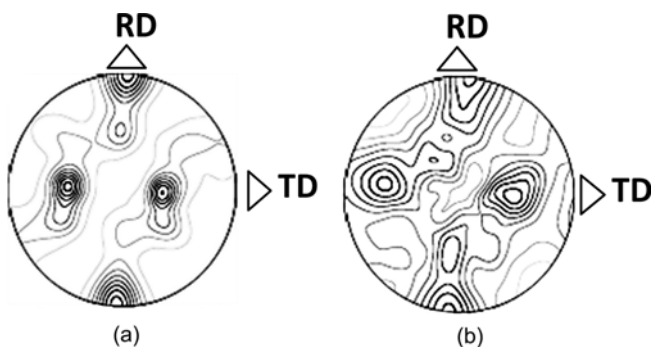


**Fig. 7.**  $\{100\}$  pole figures of (a) as-consolidated, and (b) compressed area of sample 4.

structure prior to recrystallization is uniform, with grains that are so fine their junctions are powerful pinning points. The second effect is that the cold deformation modifies the crystallographic texture. In the particular case of MA957, the increase of {111} grains with cold deformation will promote the nucleation of recrystallization.

## ACKNOWLEDGMENTS

The authors acknowledge financial support from the Spanish Ministerio de Educación y Ciencia in the form of a Coordinate Project in the Energy Area of Plan Nacional 2009 (ENE2009-13766-C04-01). C. Capdevila thanks to INCO Alloys for providing MA957, and to Prof. H.K.D.H. Bhadeshia FRS from University of Cambridge for fruitful discussions.

## REFERENCES

1. C. C. Montes and H. K. D. H. Bhadeshia, *Adv. Eng. Mater.* **5**, 232 (2003).
2. C. Capdevila and H. K. D. H. Bhadeshia, *Adv. Eng. Mater.* **3**, 647 (2001).
3. C. Capdevila, Y. L. Chen, N. C. K. Lassen, A. R. Jones and H. K. D. H. Bhadeshia, *Mater. Sci. Technol.* **17**, 693 (2001).
4. C. Capdevila, U. Miller, H. Jelenak and H. Bhadeshia, *Mater. Sci. Eng. A* **316**, 161 (2001).
5. P. Evans, J. W. Martin, E. A. Little, *Mater. Sci. Technol.* **8**, 531 (1992).
6. T. S. Chou and H. K. D. H. Bhadeshia, *Mater. Sci. Technol.* **11**, 1129 (1995).
7. H. K. D. H. Bhadeshia, *Mater. Sci. Eng. A* **223**, 64 (1997).
8. H. Regle and A. Alamo, *J. Phys. IV C7*, 727 (1993).
9. G. R. Johnson and W.H. Cook, *Proc. 7th Int. Symp. on Ballistic*, p. 541, North Holland Publishers, The Hague (1983).
10. H. Chang and I. Baker, *Metall. Mater. Trans. A* **38**, 2815 (2007).
11. B. Hutchinson and B. Wynne, *Mater. Sci. Forum* **550**, 149 (2007).
12. W. Johnson and P. B. Mellor, *Engineering Plasticity*, p. 125, Van Nostrand Reinhold, London, (1978).
13. R. C. Klug, G. Krauss, and D. K. Matlock, *Metall. Mater. Trans. A* **27**, 1945 (1996).
14. I. Toda-Caraballo, J. Chao, L. E. Lindgren, and C. Capdevila, *Scr. Mater.* **62**, 41 (2010).
15. D. M. Jaeger and A. R. Jones, *Proc. of Materials for Advanced Power Engineering* (ed. G. Coutsouradis), p. 1515, Kluwer Academic Press. Liege (1994).
16. T. S. Chou and H. K. D. H. Bhadeshia, *Metall. Trans. A* **24**, 773 (1993).